Two-dimensional crystallization of a bacterial surface protein on lipid vesicles under controlled conditions

Andreas Paul, Harald Engelhardt, Uwe Jakubowski, and Wolfgang Baumeister
Max-Planck-Institut für Biochemie, D-8033 Martinsried, Germany

ABSTRACT The solubilized surface protein of the Gram-negative bacterium *Comamonas acidovorans* was reconstituted on lipid vesicles by means of controlled dialysis. To this end, a multichamber dialysis apparatus was built which allows one to control the temperature and the dialysis rate, to apply various temperatures or buffer systems and sample conditions in a single experiment, and to monitor the turbidity of the sample by means of light scattering. The reconstitution conditions were optimized such that the surface protein formed two-dimensional crystals suitable for electron crystallography. The recrystallized surface protein arrays gave a resolution of ~1.3 nm in projection after correlation averaging of negatively stained preparations. The surface protein assembled into partially self-contained two-dimensional crystals which possess a strong shape-determining effect and formed cylinders and various cone-shaped vesicles. The development of the various vesicle forms is described in a model.

INTRODUCTION

It is a prerequisite for high-resolution electron crystallography of biological macromolecules to have two-dimensional crystals available. Recent analyses of several membrane proteins such as bacteriorhodopsin (1), the porins OmpF (2) and PhoE (3) of *Escherichia coli,* and the light-harvesting complex II of the photosynthetic apparatus (4) at near atomic resolution have become possible due to the existence or reconstitution of large and well-ordered two-dimensional crystals. Most membrane proteins have been crystallized by one of the following techniques (for recent reviews, see 5 and 6): induction of crystallization in native or reconstituted membranes by addition of ligands binding to the protein (7), lipid depletion by phospholipase treatment (8) or extraction with detergent (9), or reconstitution of the solubilized protein into lipid membranes by detergent removal (10). The latter method appears to be the most versatile and the most promising for obtaining large two-dimensional crystals of many membrane proteins.

In principle, this technique should also be applicable to proteins in which only a portion of the structure interacts with the membrane. Without sharp limit between four categories, membrane proteins may be distinguished (for a recent review see 11). The first group comprises proteins which are almost completely embedded in the membrane matrix, such as the bacterial (12) and mitochondrial porins (13), the bacterial and eukaryotic photosynthetic reactions centers (except for the bound cytochrome, 14), (bacterio)rhodopsin (15) and a number of channel-forming toxins (16, 17). Proteins which are integral in the membrane but have an appreciable portion of their mass exposed at one or both surfaces (≈60% or even more) constitute a second group. Examples of this class are transport proteins such as the transport ATPases and related enzymes (18–20) or receptor molecules like the acetylcholine receptor (21). The third group consists of (surface) proteins which are anchored to the membrane by a single transmembrane strand. Examples of this class are the M-surface proteins of Gram-positive bacteria (22), some archaebacterial surface layer proteins (23), or the integrin receptor molecules (24). The fourth group comprises surface proteins which possess covalently bound lipid. There are numerous eukaryotic and some bacterial proteins with bound phospholipid or fatty acids (25, 26) or possessing a glycolipid membrane anchor (27, 28).

The surface protein of the eubacterium *Comamonas acidovorans* which is investigated in this study belongs to group three or four of the above classification. We have applied various two-dimensional crystallization techniques to the surface protein to improve the quality and size of crystals for electron crystallography (29, 30). To study the rather strong interaction of the surface protein with the underlying membrane and its consequences for the physico-chemical properties of the membrane, it is necessary to reconstitute the protein on synthetic lipid membranes. We have used the approach of controlled dialysis originally devised for intrinsic membrane proteins (31) to crystallize the solubilized and isolated surface protein on lipid vesicles. To this end we built a multichamber dialysis apparatus which allows the exper-

Address correspondence to Dr. Engelhardt.

0006-3495/92/01/172/17 $2.00

imenter to test various crystallization parameters simultaneously and to monitor the growth of vesicles and reconstituted membranes during the experiment. Here we report on the reconstitution of the surface protein of *C. acidovorans* on DMPC vesicles and we describe the remarkable shape-determining effects the surface protein exerts on the vesicles upon crystallization.

MATERIALS AND METHODS

Preparation of the surface protein

Comamonas acidovorans, formerly *Pseudomonas acidovorans* (32) was obtained from the Deutsche Sammlung von Mikroorganismen (type strain DSM 39, identical to ATCC 15668, Braunschweig, Germany). The cells were grown aerobically in a complex medium as described earlier (33). The surface protein was isolated from outer membranes, using octyl polyoxyethylene (octyl-POE, BACHEM Heidelberg) for extraction followed by gel filtration according to the procedure described in detail by Engelhardt et al. (29). The preparation was almost free of protein impurities but contained significant amounts of lipopolysaccharides. The protein stock solution used for crystallization purposes contained 3.6 mg/ml protein in 20 mM HEPES, pH 7.0 plus 2% octyl-POE and 0.02% NaN_3.

The protein concentration was determined by the bicinchoninic acid assay according to Smith et al., (34). The concentration of the detergent was determined by depositing 10-μl aliquots on hydrophobic parafilm. The diameter of each droplet was measured by means of a video camera system magnifying the sample ~15-fold. The diameter increases approximately linearly with the octyl-POE concentration up to the critical micelle concentration (CMC ≈0.25% in 20 mM HEPES, pH 7.0). Above the CMC, the diameter is almost independent of the detergent content. The lowest concentration detectable was <0.01%. This method is essentially the same as suggested by Engel and Hoenger (unpublished results).

Electron microscopy and image processing

Purified outer membranes, protein preparations and reconstituted crystals were examined in a Philips EM 420, CM 10 or CM 12 electron microscopes using magnifications of nominally 35,000 and 39,000×. The preparations were negatively stained with unbuffered uranyl acetate (2%). Preparations embedded in aurothioglucose or in vitreous ice were imaged at liquid N_2 temperature using a Gatan cryoholder (35). We used the method described by Jakubowski and Mende (36) to produce ice films on bare copper grids which were stabilized by lipid monolayers. The quality of crystalline arrays was assessed by optical diffractometry, by computer-calculated power spectra of digitized areas and/or by correlation averaging. Areas of 1,024 pixels square were densitometered using an Eikonix 1412 camera (Eikonix Corp., Bedford, Massachusetts) with a spot size of 15 μm, corresponding to pixel sizes of 0.39 and 0.43 nm at the specimen level. The images were processed by correlation averaging (37) using the image processing system Semper 6.2 (Synoptics, Cambridge, UK) (38).

Crystallization conditions

Crystallization experiments were performed with dimyristoylphosphatidylcholine (DMPC) as the lipid throughout. 10 mg DMPC were dissolved in chloroform and dried under an N_2 stream in a glass vessel with a bottom area of ~5 cm^2. The thin DMPC film was dissolved in 20 mM HEPES pH 7.0 containing 5% octyl-POE by gentle shaking for 20 h. The final lipid concentration of the stock solution was 10 mg/ml. The lipid and protein solutions were combined such that the final protein concentration was in the range of 0.1 to 2 mg/ml and the lipid concentration was in the range of 0 to 2 mg/ml according to the requirements of the experiment. The initial octyl-POE content was adjusted to 0.5–2%. The dialysis buffer consisted of 20 mM HEPES, pH 7.0 plus 0.02% NaN_3. The dialysis experiments were usually terminated after 48–72 h.

The multichamber dialysis apparatus

In the construction of the dialysis apparatus the following design criteria were met: (*a*) several samples can be treated in a single experiment simultaneously, (*b*) the temperature control can be adjusted and held constant over a wide range, (*c*) the control of the dialysis rate can be adjusted, (*d*) the samples can be shaken gently and automatically, (*e*) the change in turbidity of the samples can be monitored during the experiment by means of light scattering, and (*f*) relevant experimental data can be stored in a personal computer.

The core of the dialysis apparatus consists of two plates made of stainless steel, 265 × 60 × 12 mm in size. The base plate (Figs. 1 and 2) contains seven holes close to the longer side where the dialysis chambers are inserted. The holes have openings towards the bottom of the plate and towards its side such that the samples can be illuminated from the side and the scattered light can be detected at an angle of 90°. The width of the slit for the incident light has been calculated such that the inner volume of the dialysis cell is completely illuminated and that total reflection does not occur. The cylindrical quartz cuvettes have an inner vol of 200 μl and possess dimensions which are close to the optimum ratio between volume and surface area (radius 3 mm, height 7 mm). The dialysis chambers are inserted into the base plate, filled with the solution containing the protein-detergent and lipid-detergent mixed micelles, and covered with the dialysis membrane (diameter 8 mm, 10–15 kDa exclusion limit). Gasket rings are layered on top and pressed onto the cuvettes by means of the top plate which is tightly screwed on to the base plate (Figs. 1 and 2). The top plate contains buffer chambers where the cuvettes are situated (volume of each buffer chamber ≈250 μl). The dialysis buffer runs through these chambers at a constant rate (≈0.3 ml/min for each chamber in most experiments). The buffer solution may be pumped through the chambers by means of a peristaltic pump or, preferably, by simply rinsing from a bottle installed ~50 cm above the level of the dialysis apparatus. The flow rate was controlled by adjusting the diameter of the tubes. Because the buffer flow is parallel, up to seven samples and/or buffer systems can be tested in a single experiment. The buffer solution is prewarmed in a water bath a few degrees above the maximum temperature used in the dialysis experiment to prevent degassing of the solution and the occurrence of air bubbles in the buffer chambers. The buffer solution is adjusted to the desired temperature during the passage through the top plate. The latter is heated or cooled by means of Peltier elements which are mounted on top, close to the ends of the plate (Fig. 1). Due to the tight contact between the top and base plates, the samples are adjusted to the desired temperature as well. The Peltier elements are individually controlled such that either a homogeneous temperature is applied to all chambers or that a temperature gradient is generated between the elements in the range of 0 to ≥50°C. Because the temperature is not ideally constant over the whole plate due to some heat loss, the effective temperature is measured in the vicinity of the dialysis chambers by a thermocouple.

To monitor the growth of vesicles and/or lipid membranes in the course of detergent removal, the cuvettes are illuminated by a UV light source with an emission maximum at 355 nm (320–400 nm major

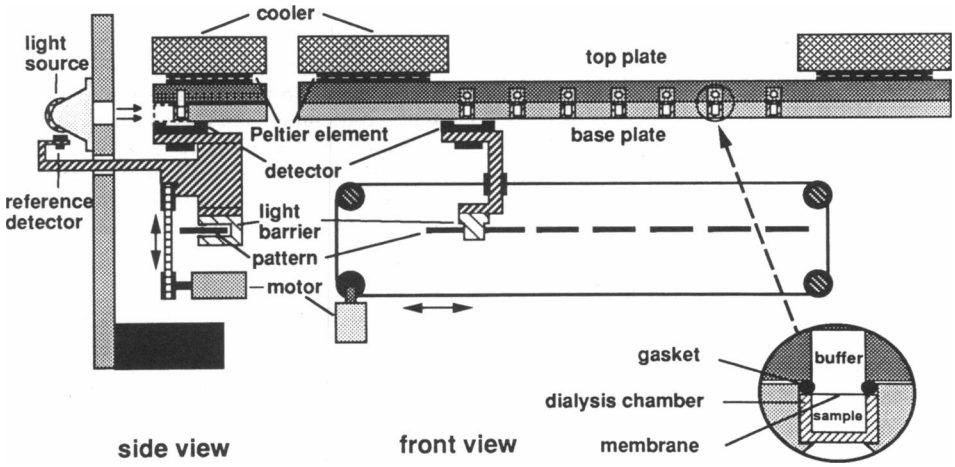

FIGURE 1 Scheme of the multichamber dialysis apparatus, viewed from the side and front. Arrows indicate the movement of the strip connected with the UV-detector element.

emission spectrum). The scattered light is detected at an angle of 90° at the bottom of the dialysis chambers by means of a UV detector. The signal is corrected for fluctuations of the light intensity by a reference detector directly measuring the emitted light at the source (Fig. 1). The detectors are moved from one chamber to the next by a motor drive in a cyclic manner; motor stops are actuated by means of a light barrier for 60 s (Fig. 1). The signals of the scattered light are stored in a personal computer and displayed as curves such that the process of vesicle formation and protein crystallization can be monitored online for each chamber. The motor of the detector as well as the temperature of the Peltier elements are controlled by the computer. Thus, time-dependent and parameter-dependent temperature programs can be applied, e.g., an initial heating phase or a final cooling phase as well as cyclic temperature shifts of one or both Peltier elements. To prevent sedimentation of vesicles and to support gentle mixing of the samples during the experiment, the plates are mounted on a frame with

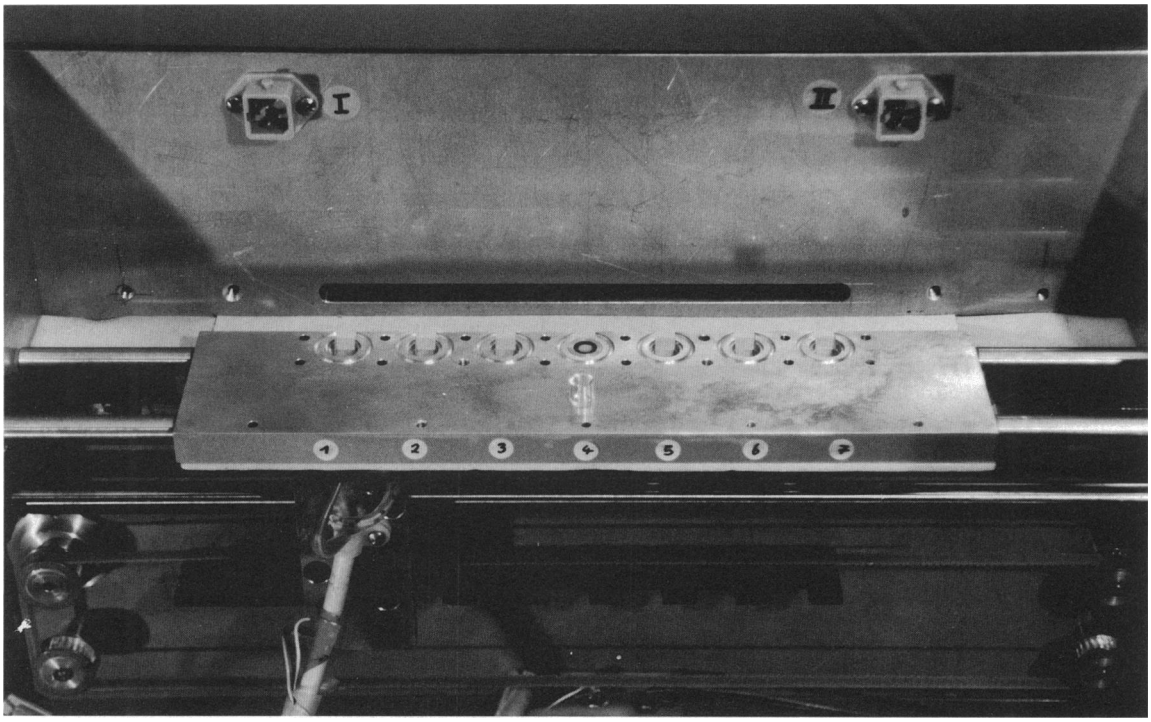

FIGURE 2 The multichamber dialysis apparatus. The base plate contains seven holes for the dialysis chambers, i.e., quartz cuvettes (position 4).

semicardanic construction. The plates are moved around a horizontal axis with a frequency of ~ 5–$10\ min^{-1}$ and an angle of $\sim \pm 60°$.

RESULTS

Information from light scattering curves

Light scattering curves were recorded to monitor the formation of lipid vesicles and their interaction with the solubilized bacterial surface protein. The dialysis experiments show three characteristic phases according to the scattering curves (Fig. 3). The initial phase is characterized by a rather slow increase of the relative scattering intensity. The length of this "lag-phase" depends on the initial concentration of the detergent, which was octyl-POE in our experiments. It was usually not longer than ~ 10 h with octyl-POE concentrations in the range of 0.5–0.7%. The second phase shows a rapid change of the scattering signal. It can be correlated with the formation and growth of vesicles formed from mixed micelles in the course of detergent removal. The signal may be approximated by Rayleigh scattering (valid for solid, homogeneous spheres) where the scattering intensity is critically dependent on the particle size for a given wavelength λ. This holds true up to a diameter of $\approx \lambda/10$ (39) which corresponds to ~ 30–40 nm. A characteristic for the third phase is an almost constant signal, apparently decreasing over two to five days (Fig. 3 *c*). This slow decrease is typical for particles of increasing size (diameter $\geq \lambda$) and is appropriately described by the theory of Mie scattering (Fig. 3 *a*), especially if a heterogeneous population of particles with a certain size distribution is assumed rather than a constant vesicle diameter (40). The light micrographs in Fig. 4 illustrate the size distribution of the vesicles obtained in various experiments. The largest vesicles were $\approx 20\ \mu m$ in diameter.

Control experiments using solubilized DMPC but omitting the protein revealed the reproducible formation of vesicles. The relative scattering intensities were clearly below those of samples containing vesicles covered with densely packed or crystalline protein (Fig. 3 *b*). Obviously then, the scattering curves also provide information on the reconstitution of the surface protein.

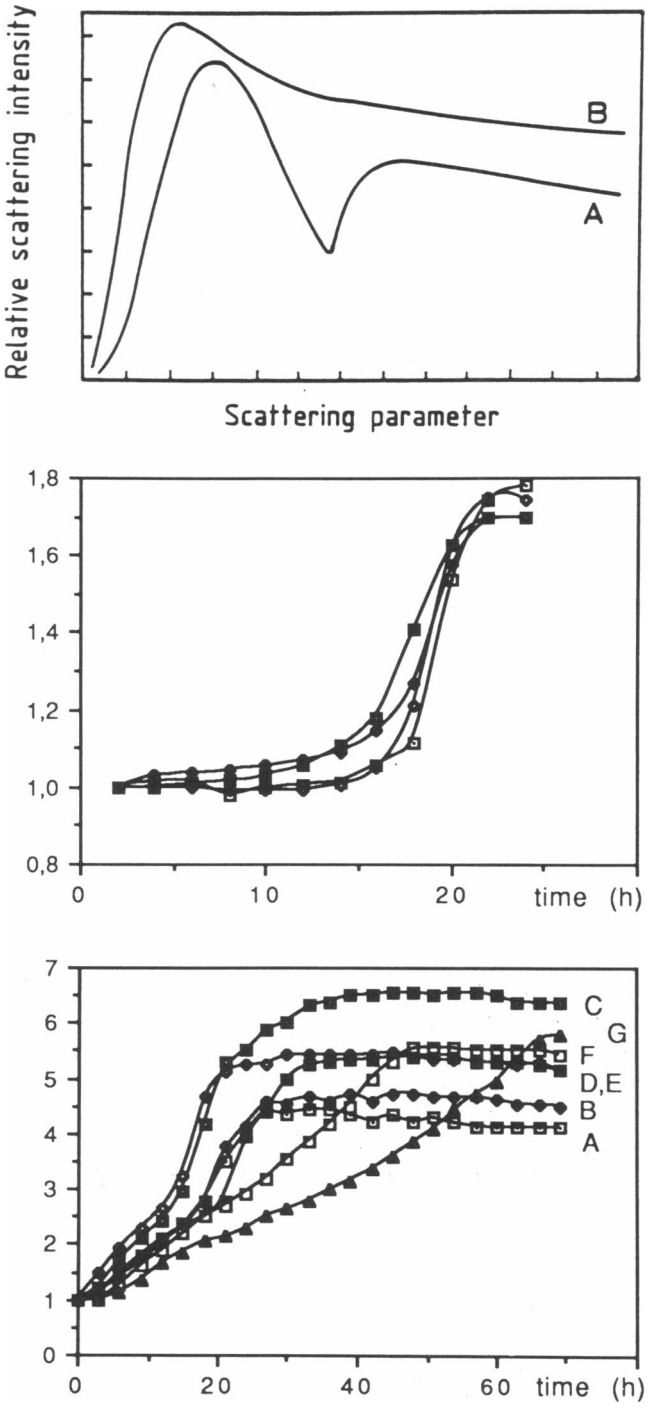

FIGURE 3 Light scattering curves showing the relative scattering intensity as a function of the scattering parameter (*a*) and of the time (*b*, *c*) in the case of dialysis experiments. (*a*) Theoretical scattering curves calculated by means of the Mie scattering theory using a scheme adapted from Foitzik and Hinzpeter (40). Curve *A* illustrates the scattering signal obtained from spheres of a certain radius *r* and curve *B* derives from a population of spheres with an average radius *r* and a certain standard deviation (Gaussian distribution). Scattering parameter = $2\pi r/\lambda$. (*b*) Empirical scattering curves obtained in a dialysis experiment with DMPC at 37°C but with no protein present. The four curves derive from identical samples illustrating the reproducibility of the dialysis kinetics. (*c*) Scattering curves of a dialysis experiment performed at 30°C, with 1 mg/ml surface protein and DMPC concentrations (mg/ml) as follows; the initial octyl-POE concentration (%) is given in brackets. (*A*) 0 (0.5%), (*B*) 0.05 (0.52%), (*C*) 0.1 (0.55%), (*D*) 0.25 (0.63%), (*E*) 0.5 (0.75%), (*F*) 1.0 (1.0%), (*G*) 2.0 (1.5%). All the samples contained residual lipid (lipopolysaccharides).

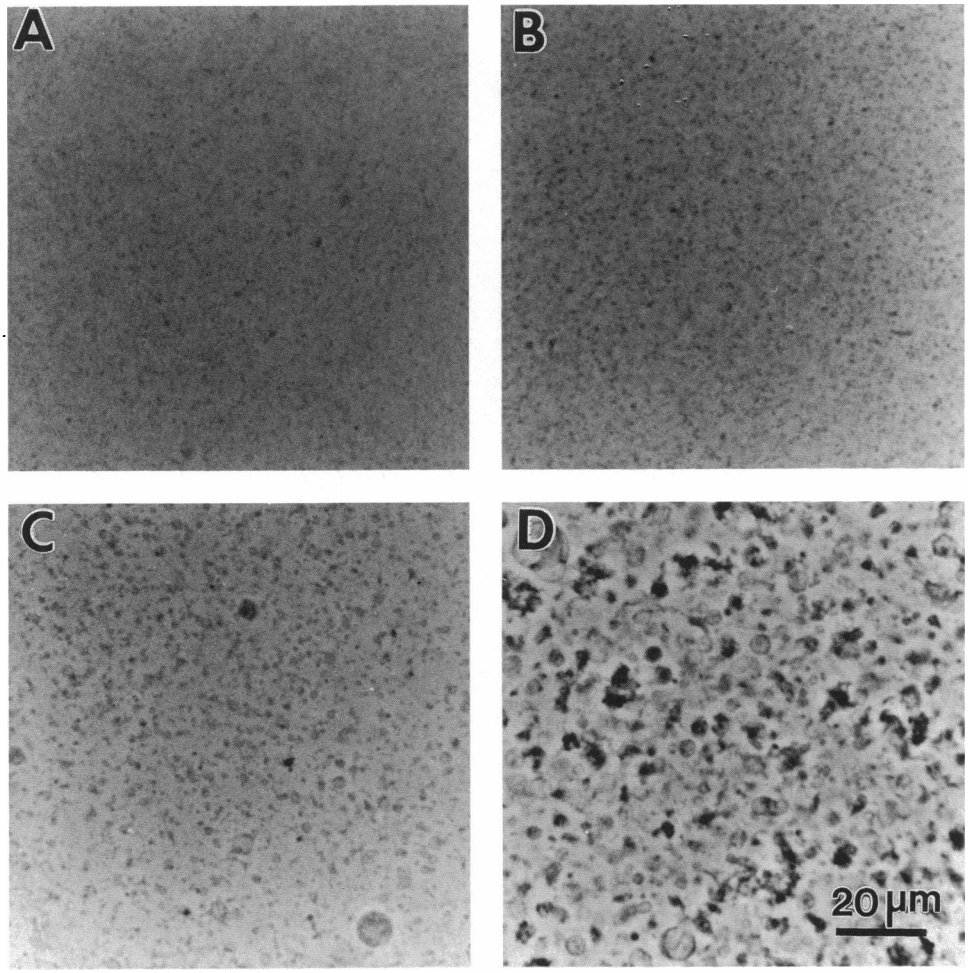

FIGURE 4 Light microscopical images of vesicles obtained from dialysis experiments at various temperatures. (*A*) 27°C, (*B*) 31°C, (*C*) 35°C, (*D*) 40°C, protein concentration 1 mg/ml, DMPC 0.5 mg/ml.

Optimizing the reconstitution conditions

The following parameters which were expected to have an influence on the vesicle formation and crystallization processes have been optimized: the lipid-to-protein ratio, the initial octyl-POE concentration, and the temperature. The lipid-to-protein ratio was varied between 0 and 5 (w/w), using a constant protein concentration of 1 mg/ml and a constant temperature of 30°C. The (maximum) size of vesicles increased with the lipid content from 0.3 μm in diameter (0.05 mg DMPC/ml) to 1 μm (0.1 mg DMPC/ml), 5 μm (0.25 mg DMPC/ml) and ≈20 μm (≥0.5 mg DMPC/ml) as judged by light and electron microscopy. The smaller vesicles turned out to be almost completely covered with protein, either densely packed but unordered or regularly arrayed, whereas the larger vesicles frequently showed areas apparently free of protein. All the samples contained excess soluble protein not attached to the lipid vesicles. The optimum lipid to protein ratio with respect to the size of crystalline patches was 0.5 mg/ml DMPC to 1 mg/ml surface protein with an initial octyl-POE content of 0.5 to 0.6%. The experiments described below were performed under these conditions.

The temperature proved to be a very important parameter for vesicle and crystal formation. The micrographs in Fig. 4 illustrate the size distribution of vesicles formed in a dialysis experiment at different temperatures. An increase from 27 to 35°C resulted in a continuous increase of the vesicle size, and a drastic increase was observed between 35 and 40°C. The average diameters of the vesicles shown in Fig. 4 were ~0.5–0.8 μm (27°C), 1.1 μm (31°C), 1.6 μm (35°C), and 3–4.5 μm (40°C).

Effects of the dialysis temperature

Crystallization of the *C. acidovorans* surface protein occurred at temperatures between 9 and 45°C but with significant differences in the size and quality of the regular arrays and in the size and shape of the vesicles. Reconstitution experiments below 30°C yielded neither large vesicles, corroborating the observations documented in Fig. 4, nor large two-dimensional crystalline arrays. The diameters of the vesicles were between 0.1–0.3 μm (9°C), 0.1–0.4 μm (17°C), and 0.2–0.6 μm (28°C). The surface protein was clearly attached to the spherical DMPC vesicles at 9°C but only a few small regular arrays were observed. There was no significant change around 23°C, i.e., the phase transition temperature of pure DMPC membrane systems. However a drastic improvement of the two-dimensional crystallization was observed between 30 and 40°C. Fig. 5 shows a low magnification micrograph of a characteristic preparation of vesicles found in a dialysis experiment at 37°C. Three classes of vesicle forms were found: (*a*) spherical vesicles of various sizes, (*b*) cylindrical forms of variable widths and lengths, and (*c*) vesicles with a spherical and a cone-shaped portion. The spherical vesicles and the spherical portions of cylindrical (Fig. 6) and cone-shaped (Fig. 7) forms were almost completely covered with the surface protein forming patches of two-dimensional crystals but the protein only rarely formed large regular arrays. The cylindrical and conelike portions, however, were apparently completely crystalline except for the pole caps. Fig. 6 shows a gallery of characteristic cylindric forms. The cylinders were usually 0.7 to 3 μm in length and 0.3 to 0.8 μm in width. Sometimes extremely long cylinders were observed (5 to 10 μm or even longer). We found single cylinders (Fig. 6 *C*) and forms which appear to originate from a (formerly) spherical vesicle (Fig. 6, *A* and *B*). The finger-like variant in Fig. 6 *A* occurred rarely.

Three types of cone-shaped vesicles were observed: acute-angled (45°), right-angled, and obtuse-angled (135°) forms (Figs. 5 and 7) the frequency of occurrence decreasing in this order. The cones, again, were less frequent than cylindrical variants. These geometric forms gave double-layered two-dimensional crystals as judged from the existence of Moiré patterns and from (light

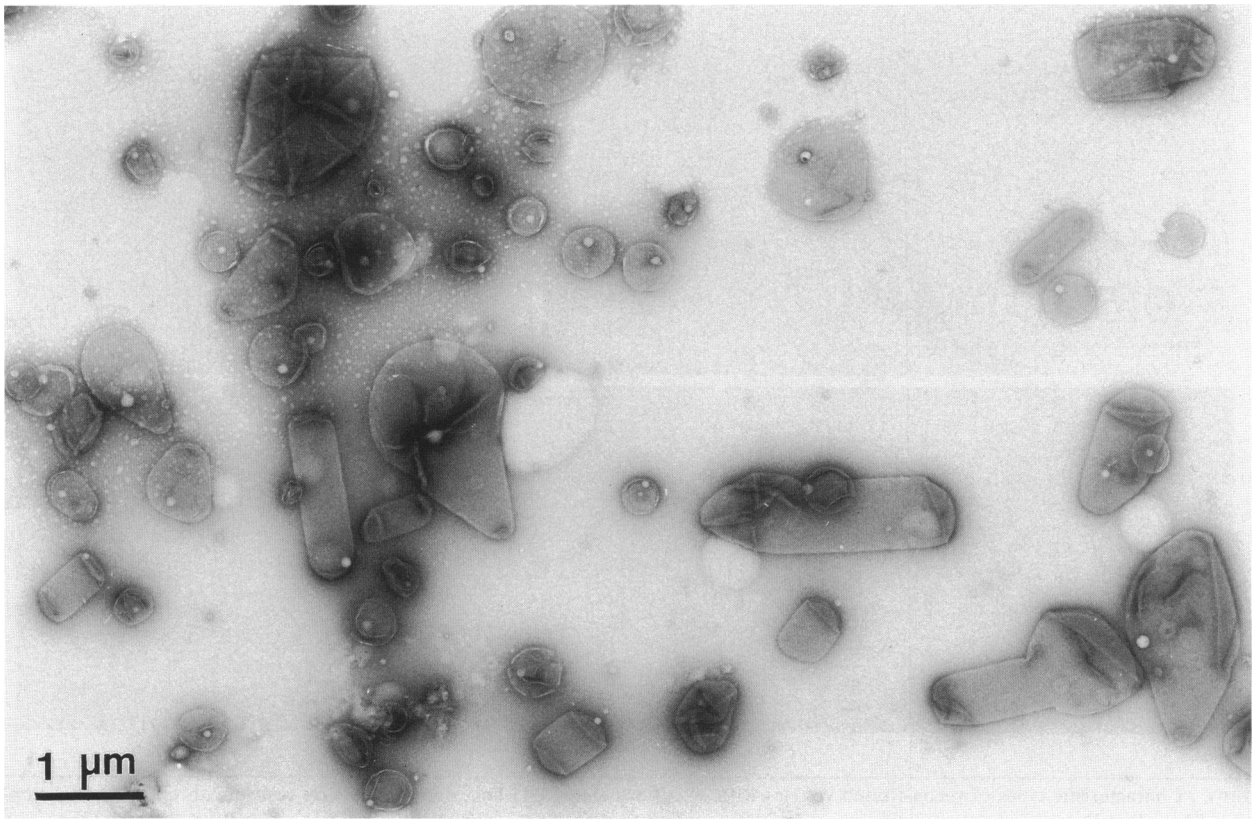

FIGURE 5 Electron micrograph of vesicles obtained from a reconstitution experiment performed at 37°C. Concentration of surface protein = 1 mg/ml, of DMPC = 0.5 mg/ml.

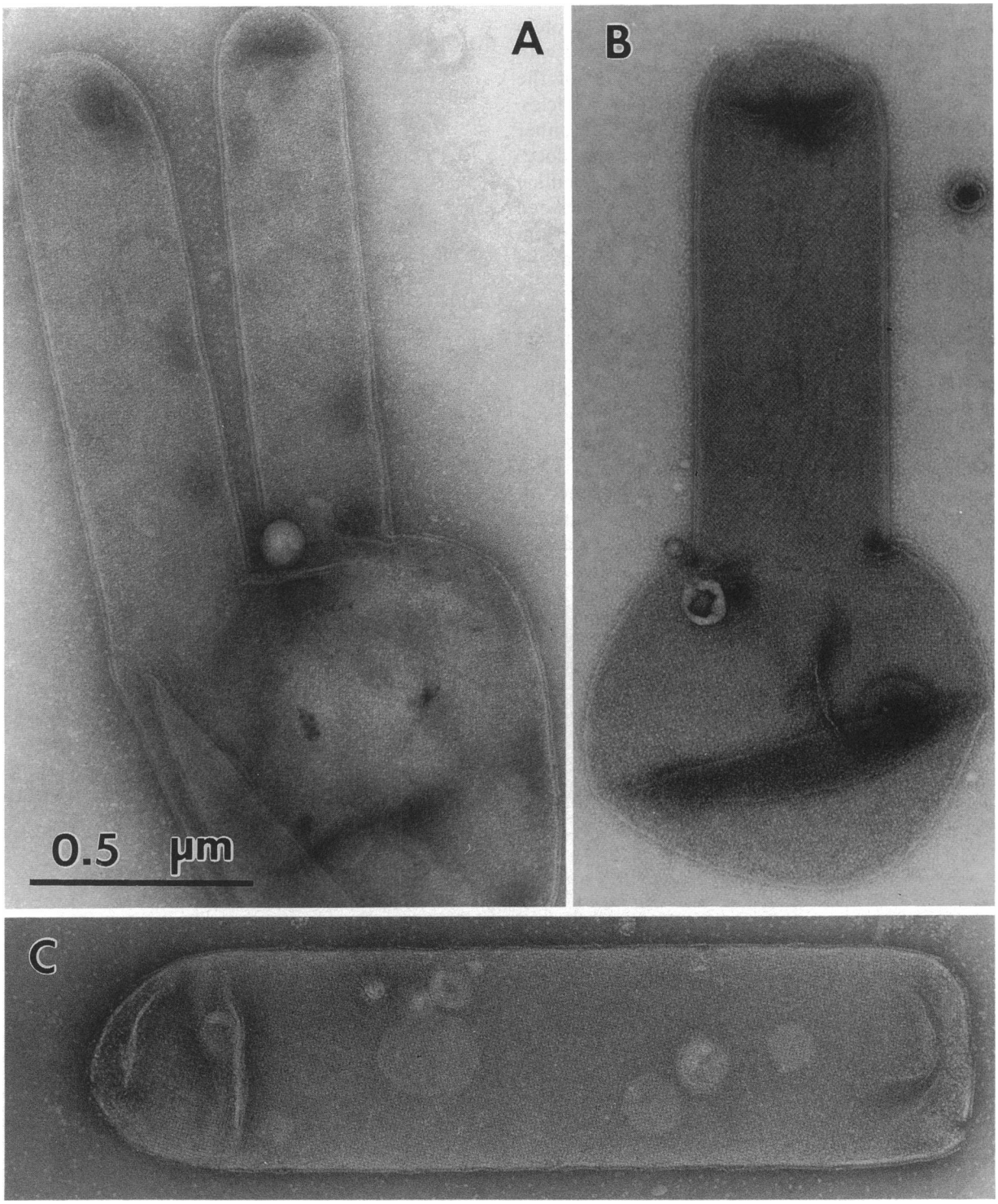

FIGURE 6 Characteristic types of reconstituted vesicles with cylindrical shape (*A*) fingerlike vesicle, (*B*) vesicle with cylindrical portion. (*C*) cylinder. The cylindrical forms are completely covered with the surface protein, showing two lattices originating from the upper and the lower side of the flattened vesicles. The continuous layer of the surface protein is particularly well detectable at the edges of the vesicles where the outer line represents the surface protein and the lighter, inner line the edge of the lipid vesicle.

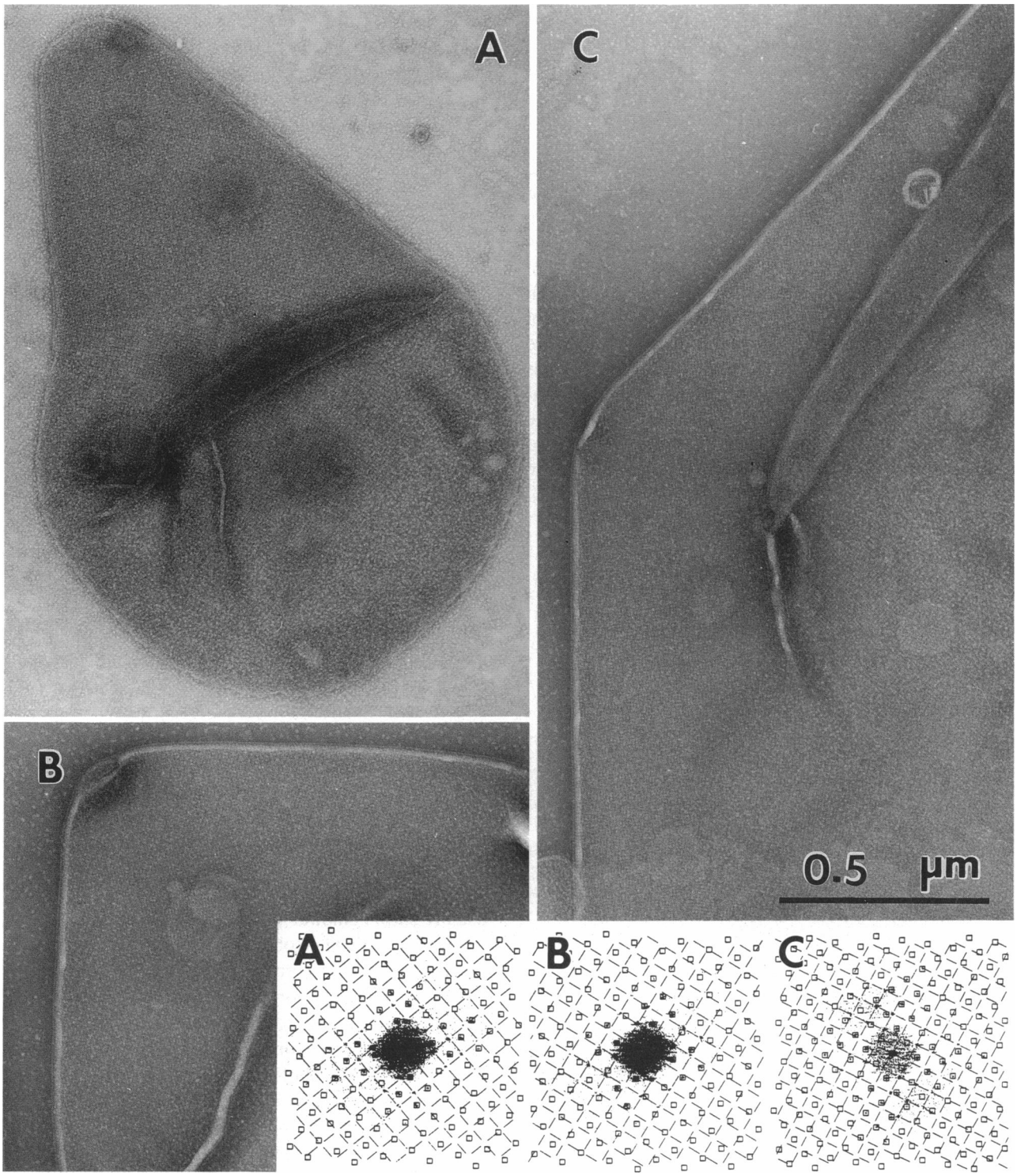

FIGURE 7 Characteristic types of reconstituted vesicles with conelike shape, here flattened cones which possess the characteristic angles of (*A*) 45°, (*B*) 90°, and (*C*) 135°. The conelike portions are completely covered with the crystalline surface protein, showing two lattices originating from the upper and the lower side of the vesicle. Insets: power spectra from the cone-shaped regions in which the spectra of the two lattices are marked by lines and boxes.

optical) diffractograms (Fig. 7), whereas the spherical vesicles also showed single-layered crystals. A closer analysis of the cylinders and cones consistently revealed the following characteristics. First, the diffractograms indicate that there are two, and only two, lattices rotated with respect to each other, originating from the upper and the lower side of the (flattened) vesicles; second, image analysis, using cross correlation techniques to find the actual positions of the unit cells, revealed that the (flat) lattices are homogeneous and do not contain dislocations or disclinations (Fig. 8). Some lattice distortions originating from flattening effects and deviations of the correlation peaks from the positions of an ideal lattice do exist of course, but discontinuities have not been observed. Third, the upper and lower lattices are also continuous and, thus, the two-dimensional crystals are (partly) self contained. Fig. 8 shows that the orientations of the two lattices are apparently reflected at the edges of the flattened cone. This property is expected from continuous lattices (of any symmetry) which are folded over and is independent of the orientation of the lattice with respect to the folding edges. We indeed found arbitrary angles between the lattice and the edges but consistently observed the reflection effect with all the cylinders and cones analyzed.

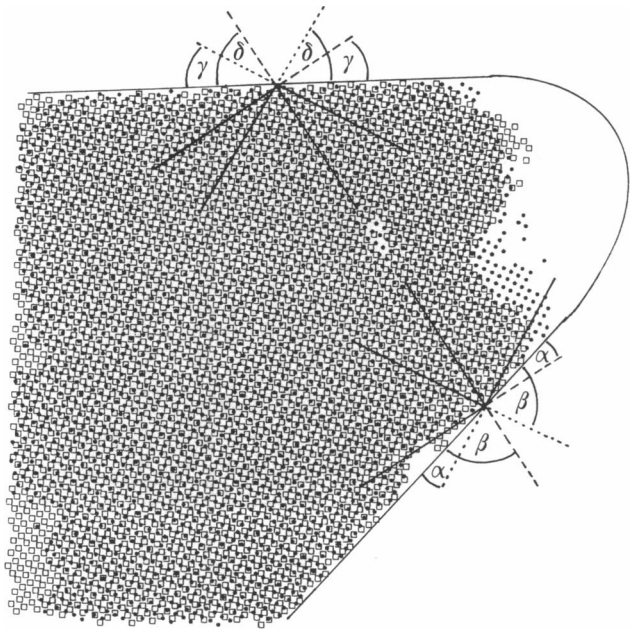

FIGURE 8 Unit cell positions of the two superimposed lattices (lower *, upper □) of the flattened cone-shaped portion of the vesicle shown in Fig. 7*A* (rotated by 90° here). The image was Fourier-filtered such that the two superimposed lattices were separated. The back-transformed images now contained the lower and the upper lattices isolated. Reference areas of four unit cells in size each were extracted and cross-correlated with the original image. The positions of the unit cells were determined in the two cross-correlation functions and superimposed afterwards. The lines indicate the orientations of the lower (· · · · ·) and the upper (---) lattices and the angles (α, β, γ, δ) illustrate that the orientations of the lattices are apparently reflected at the vesicle borders.

The shape-determining effect of the two-dimensional crystals requires that the surface protein interacts strongly with the lipid membrane. This could be demonstrated by means of vesicles which were embedded in vitreous ice or in aurothioglucose and imaged by cryo-electron microscopy. The vesicles are not ideally round in the *z*-direction because of the limited thickness of the water film (~0.4 μm), but there are no adsorption effects because the water film was spanned over holes of the grid and was not supported by, e.g., a carbon film. Fig. 9 clearly shows that the vesicles are flattened where the protein crystals are attached, even if the crystals were not self contained. The crystal of the surface protein is obviously more rigid than the lipid vesicle which is forced to change its shape.

Structure of the reconstituted surface protein

The reconstituted crystals in most cases gave a higher resolution in light-optical diffractograms and after correlation averaging than the original regular arrays on the bacterial outer membranes. Correlation averages of a reconstituted crystal and a natural regular array are displayed in Fig. 10. The average of the recrystallized surface protein has, according to the radial correlation function criterion (37), a resolution of ~1.3 nm which corresponds to the practical limit of negative staining (41). Using the same criterion a resolution of ~1.7 nm was obtained with the native outer membrane which usually shows smaller patches of two-dimensional crystals and a somewhat obliterated structure in projection due to the complex composition of the outer membrane. The morphological complexes have the same architecture in the native lattice and in reconstituted crystals and the unit cell dimensions are identical (lattice constant 10.5 nm). The morphological complex is a dimer (29, 30) characterized by two units of mass. As indicated in Fig. 10*A* the major mass possesses a small side lobe which is less clearly seen in Fig. 10 *B*. This mass presumably represents the domain pointing towards the membrane and mediating the tight contact as suggested from a three-dimensional reconstruction of the surface protein (30). This illustrates the excellent preservation of the structure of the surface protein attached to the DMPC membrane.

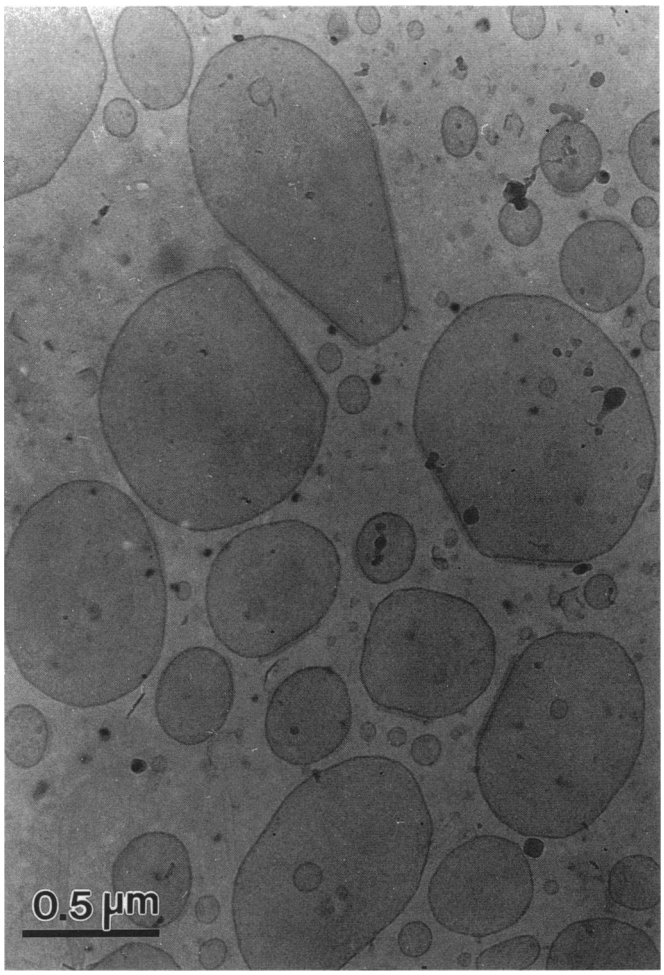

FIGURE 9 Frozen hydrated, unstained preparation of reconstituted vesicles imaged by means of cryo-electron microscopy. The vesicles are deformed where the crystalline surface protein is attached, indicating a strong interaction between the surface protein and the lipid membrane.

DISCUSSION

Detergent removal by means of dialysis is the method of choice for two-dimensional crystallization of solubilized membrane proteins. Simple dialysis has been applied successfully to a variety of proteins, e.g., the light-harvesting a/b complex (42, 43) and the bacterial photosynthetic reaction center (44). In an experimental variant, lipid-detergent mixed micelles are added to support the formation of membranes and/or vesicles containing the regular protein arrays. The cytochrome reductase was the first protein complex crystallized by this technique (10) and was followed by a number of other membrane proteins (5). We have used this approach to reconstitute the surface protein of the bacterium *Comamonas acidovorans* on DMPC vesicles. The protein is not a typical intrinsic membrane protein but is tightly associated with the outer membrane of the bacterial cell and is probably anchored to it by a small hydrophobic domain (29, 30). Therefore, the surface protein can be treated like an intrinsic membrane protein in two-dimensional crystallization experiments. The successful crystallization indicates that other surface proteins may also be reconstituted by controlled dialysis, e.g., the M-proteins of Gram-positive bacteria (22), surface layer proteins of archaebacteria, possessing membrane anchors (23), and molecules such as integrin (24) as well as those proteins containing covalently bound (glyco)lipid or fatty acid molecules (25–28). This technique is an alternative which may be especially useful for proteins which are not water soluble enough to be crystallized by the lipid monolayer approach (45) or on mica (46).

Controlled (rapid) dialysis by means of a flow-through dialysis system was first used for the production of lipid

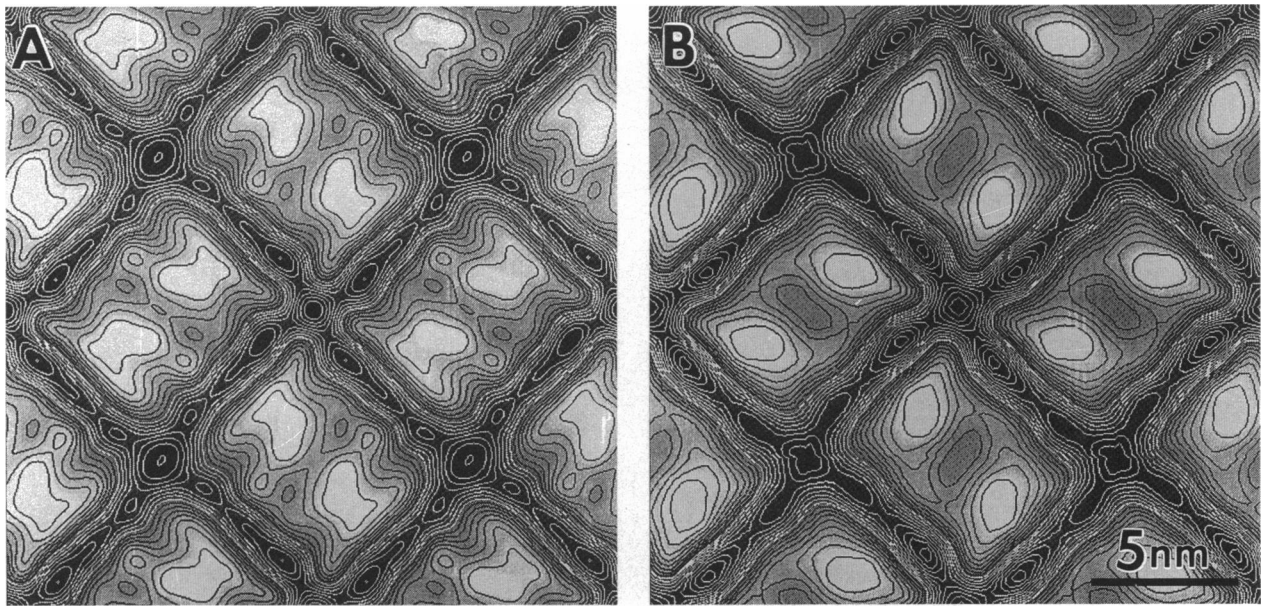

FIGURE 10 Correlation averages of negatively stained preparations of (*A*) a crystal reconstituted on a DMPC vesicle and (*B*) the native layer of the surface protein of *C. acidovorans*. Lattice constants 10.5 nm, resolutions according to the radial correlation function criterion (*A*) 1.3 nm, (*B*) 1.7 nm.

vesicles (47) and was recently adapted for two-dimensional crystallization purposes by Engel et al. (31). Our experimental setup described here introduces new features which are particularly valuable for optimizing the crystallization conditions. First, up to seven samples can be treated independently in a single experiment; this is of advantage for testing various buffer systems, lipids, concentrations, et cetera. A series of experiments would otherwise be extremely time consuming. Second, the application of temperature gradients allows one to run experiments at different temperatures simultaneously. The dialysis temperature indeed proved to be an important parameter for two-dimensional crystallization. Third, the scattering curves provide information on the growth of vesicles and, thus, indirectly on the kinetics of detergent removal, which is dependent on the initial detergent concentration. The experiments can be terminated when the dialysis appears to be complete. Finally, the reconstitution of the surface protein amplifies the scattering intensity two- to four-fold or even more relative to the scattering power of DMPC vesicles free of protein. This is presumably due to the formation of a protein shell on the lipid vesicles changing the apparent refractive index. (Analytical solutions of this complex scattering problem were given by Aden and Kerker for a special case, 48). This property provides a valuable tool for judging the success of reconstitution experiments. Of course, to determine if crystallization has occurred, the samples must be examined in the electron microscope.

The vesicles, pure DMPC vesicles as well as those carrying regular arrays of the surface protein, apparently increase in size during the entire dialysis experiment, according to the scattering curves which show the characteristic decline of Mie scattering with particles of nonhomogeneous diameter (40). We assume that fusion of spherical vesicles and those possessing a spherical portion is involved in formation of large vesicles, especially at higher temperatures. This could explain the occurrence of peculiar vesicle forms. However, the details of vesicle development and the dialysis kinetics remain to be investigated; it is a drawback of our dialysis apparatus that samples cannot be taken during the experiment without interrupting it.

For electron crystallography and electron diffraction in particular large and well ordered two-dimensional crystals are required. Important parameters for obtaining large lipid vesicles are (*a*) the dialysis rate, (*b*) the lipid-to-detergent ratio (49), (*c*) the total lipid content, and (*d*) the pH-value (49). To our knowledge there is little information on the effect of temperature on the size of liposomes obtained in dialysis systems. It is, however, apparent that the critical temperature of phase separation is important for the clustering of micelles (50). The three-component system lipid-detergent-protein, containing mixed lipid-detergent and protein-

detergent micelles or complexes, respectively, is much more complex with respect to the parameters mentioned above. In trying to obtain suitable crystals for electron microscopy we found that the initial molar lipid-to-detergent ratio of 1:20 is in the optimal range with 0.5 mg/ml DMPC and 1 mg/ml surface protein at pH 7.0 and 30–40°C. Neither the ionic milieu nor the pH-value have been optimized experimentally, yet we observed significant effects due to the changes of the dialysis temperature. With increasing temperatures the size of the vesicles as well as the size of the two-dimensional crystals increased. There was no obvious change near the phase-transition temperature of 23°C for DMPC, but we obtained a drastic change of the crystallization behaviour >30°C. It is difficult to correlate this particular temperature with known properties of the lipid because the buffer components, the detergent, residual lipopolysaccharide and the protein do exert an influence on the phase behavior of the vesicles which remains to be investigated in detail. Another possibility is to relate the temperature effects to an activation energy which is necessary to form nucleation sites of sufficient size for crystallization. Suitable temperatures for two-dimensional crystallization appear to be ≥ 20°C for many proteins and surfactants without additional lipid present (42–44) and 25–37°C for protein-lipid systems like the bacterial porins (31, 51), the cytochrome reductase (52), and the surface protein investigated here. It is obvious that the type of detergent and, in particular, the length of its hydrophobic tail is an important parameter (50).

The occurrence of the peculiar vesicle forms, cylinders and the various cones, might be due to the following properties of the DMPC-surface protein system: (*a*) the capability of the DMPC vesicles to assume various forms other than spherical, a property which is temperature dependent (53) and might contribute to the temperature effect observed, (*b*) the strong interaction of the surface protein with the lipid membrane which is probably mediated by a membrane anchor (29, 30), (*c*) the relative rigidity of the protein crystal which has been demonstrated with frozen specimens showing that the vesicles are flattened where the two-dimensional crystals are attached, and (*d*) the formation of partially self contained regular arrays which give rise to and stabilize the particular forms observed.

The fact that the two-dimensional crystals are capable of forming (partly) self contained and continuous envelopes provides the key for understanding the architecture of the vesicle forms. The model in Fig. 11 *A* illustrates how a cylinder and cones can be obtained from a tetragonal lattice. The mechanism may be described in terms of disclinations where a certain piece of the two-dimensional crystal is removed and the free crystal edges are related by rotation such that new bonds

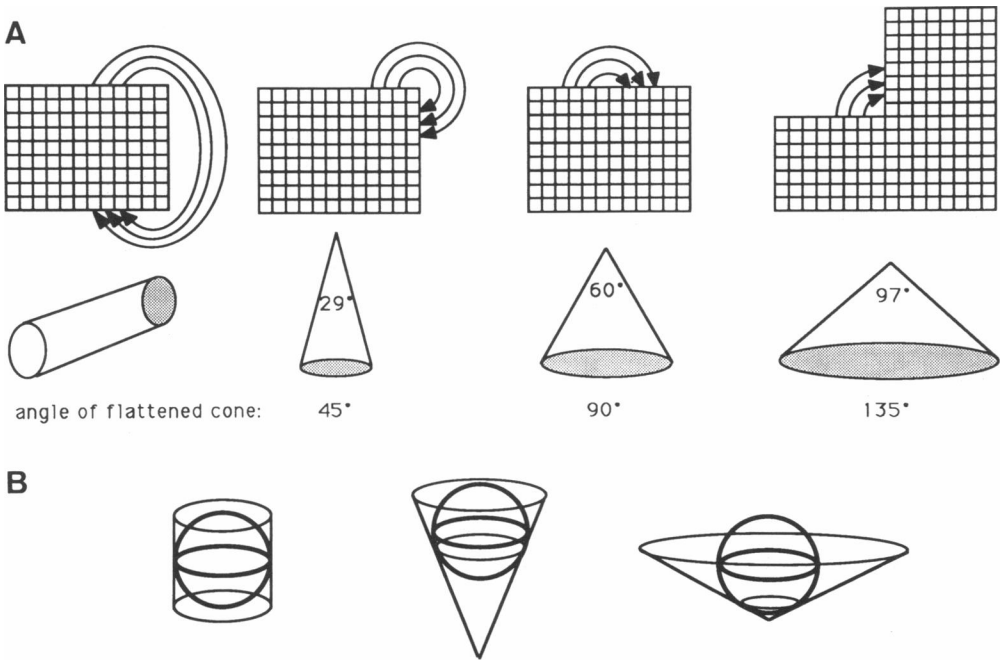

FIGURE 11 (*A*) Scheme of the construction of a cylinder and cones by a tetragonal lattice. (*B*) Model for the development of a cylinder and cones on a spherical vesicle. Bold lines indicate the shape and equator of the sphere, whereas the normal lines outline the cylinder and cones and the contact zones on the sphere on a parallel to the vesicle equator.

among the aligned unit cells can be formed. This method corresponds to the Volterra process describing the construction of dislocations and disclinations (54). Apparent 360° "disclinations" as well as 270°, 180° and even 90° disclinations are impossible or at least highly unstable in the plane of a two-dimensional crystal. The stress energy forces the crystal to assume a shape resulting in a relative minimum deformation of each bonding. If the two-dimensional crystal is flexible and not attached to a rigid support, it is bent out of plane. Cylinders and cones are geometric forms characterized by a minimum (ideally no) deformation of the two-dimensional crystal within the curved surface (Fig. 11 *A*). The cones expected for a lattice of p4-symmetry possess (undistorted) solid angles of 28.96°, 60°, and 97.18° corresponding to the angles of the flattened cones of 45°, 90°, and 135° which were indeed observed. This principle also applies for crystals with other symmetry properties; the geometric forms possible for the 17 plane groups of two-dimensional crystals are listed in the Appendix.

The model introducing disclinations does explain the existence of the particular forms observed but not why the crystals create a cylinder from one vesicle and a cone from another. The scheme shown in Fig. 11 *B* illustrates (ignoring the flattening effect of attached crystals) that cylinders may be formed if the crystals grow approximately around the equator of the vesicle while cones arise if the crystals grow subequatorial on a parallel of latitude. Acute-angled cones occur if the growing zone is on a parallel close to the equator whereas obtuse-angled cones appear on parallels closer to the vesicle poles. Whether a single crystal grows around a vesicle or, more likely, the large crystal is a fusion product of smaller patches remains to be established. Although the crystallization kinetics have not been investigated in detail here one can conclude from the diameters of the cylinders (0.3–0.8 μm) that the formation of self-contained crystals must occur at a later state of vesicle development. To obtain two-dimensional crystals as large as possible the formation of self-contained crystals should not happen to early with respect to the growth of the lipid vesicles. We can conclude from our experiments that the optimization of the lipid-to-protein ratio and of the temperature are necessary to adjust the kinetics of vesicle development and crystal growth such that an optimum coverage of the lipid with protein and a maximum size of the vesicles are obtained. Further parameters, e.g., the ionic milieu and the pH value, may also be of importance of course.

The quality of the (self contained) lattices is apparently good as judged from correlation averages. The resolution achieved (1.3–1.5 nm) is close to the limit of negatively stained preparations (41) and promises to be substantially better with crystals embedded in (aurothio)-glucose and imaged by cryo-electron microscopy. These experiments are in progress. Moreover, the reconstituted crystals can now be used to investigate the surface protein-lipid association and its consequences for the phase behavior of the membrane in more detail.

TABLE A1 Naturally occurring partially self-contained two-dimensional crystals (cylinders) of biological macromolecules

Species	Type of macromolecule	Diameter of cylinder	Symmetry	Lattice spacing (nm)	Reference
Archaebacteria					
*Thermoproteus tenax**	Surface layer	0.4 μm	p6	32.8‡	A15
T. neutrophilus	Surface layer	0.35 μm	p6	30.6	A14
Pyrobaculum islandicum	Surface layer	0.43 μm	p6	29.9	A16
P. organotrophum	Surface layer I	0.4 μm	p6	27.9	A17
	Surface layer II		p6	20.6	
Methanospirillum hungatei	Sheath	0.5 μm	p2†	$a = 5.6, b = 2.8$ $\gamma = 86°$	A18
Methanothrix concilii§	Sheath	0.8 μm	p2	$a = 5.6, b = 2.8$ $\gamma = 86°$	A19
Eubacteria					
Caulobacter crescentus	Surface layer	0.1 μm	p6	23.5	A20
Thermophile species (stalk)	Porin	0.07 μm	p3	9.2	A4
Halophile species (stalk)	Porin	0.12 μm	p3	9.0	A5
Thiocapsa pfennigii	Photosynthetic unit	0.036 μm	p6	12.6	A7
Escherichia coli (HB101)	Fumarate reductase	0.027 μm	hexagonal	6.6	A21
Gram-negative bacterium	Spinae	0.06 μm	(p1?)	($a = 11, b = 5.7$)	A22
Anabaena flos-aquae‖	Gas vesicle	0.085 μm	(p1?)	($a = 4.57, b = 1.15$)	A23

*Presumably also valid for *T. uzoniensis* (A24); ‡31.4 nm according to (A14); †p1 symmetry according to (A25), $a = 12$ nm, $b = 2.9$ nm, $\gamma = 93.7°$; § synonymus with *M. soehngenii* (A26); ‖various diameters with other species (A27), lattice spacings mean orthogonal distances.

APPENDIX

Geometric forms of partially self-contained two-dimensional crystals of biological macromolecules

by Harald Engelhardt

Two-dimensional crystals of biological macromolecules are not ideally plane in natural systems but curved. They usually appear attached on the cell envelope, e.g., surface layers of many eubacterial and archaebacterial species (A1–A3), or they represent integral membrane proteins, e.g., regularly arrayed porins (A4–A6) and crystalline photosynthetic membranes (A7). The capacity to create curved surfaces may be an inherent property of the molecules (A8, A9).

A special case of naturally occurring two-dimensional crystals are those forming a (partially) continuous lattice around the cell or a subcellular structure, i.e., partially self-contained crystals. They possess a strong shape-determining effect like the regularly arrayed porins of the bacterial stalks (A4, A5), and they may even conserve a particular diameter of bacterial cells from one generation to the next. Remarkable examples are the surface layers of some archaebacteria (Table A1). Further cylindrical structures formed by proteins are the gas vesicles and the spinae of bacteria (Table A1). It is, thus, of interest to evaluate the potential of two-dimensional crystals to form self-contained lattices and to investigate the properties of the building blocks, i.e., the macromolecular complexes, which create the regular arrays.

The crystallization studies performed with the tetragonal surface protein of *Comamonas acidovorans* revealed that cylindrical and cone-shaped self-contained crystals may occur (A10). The cylinders as well as the cones may theoretically be constructed by the Volterra process (A11) introducing disclinations. This process is followed by another step where the stress energy in plane is transformed resulting in deformation of the whole lattice such that the crystal bondings and the unit cells are only bent out of plane (see Paul et al. (A10) for a schematic outline of the procedure). Table A2 summarizes the geometric forms which are possible for the 17 plane groups of two-dimensional crystals. The following conclusions can be drawn.

First, the number of the principle symmetry coincides with the number of different forms that can be obtained (for simple mathematical reasons). Second, the geometric forms are cylinders and cones (of different angles); cylinders can be formed in each plane group. Third, two types of cylinders are to be distinguished with p1 and p2 symmetries (and two types of 60° cones with the p2 symmetries) due to the fact that the lattice vectors a and b are of different lengths. (There are even more possibilities to form cylinders and equivalent cones with the other symmetry groups but because $b = a$ here they are indistinguishable.) Fourth, the forms which can be obtained for a certain plane group in practice depend on the particular configuration of the building block. All the forms can be obtained in any case if the monomer (the asymmetric unit) or the crystallographic unit cell represent the crystallization complex. The latter is, however, impossible in practice with plane groups where the borders of the unit cells cross the molecules (e.g., plane group $p22_12_1$ illustrated in Fig. A1)—for a compilation of the various unit cells see, e.g., (A12, A13). The evaluation of all the building blocks possible (not larger than of unit cell size) for each plane group reveals that the forms listed in Table A2 may also be obtained from crystallization complexes which are smaller than of unit cell size, e.g., ½ for p2-related symmetries, ⅓ for p3, ½ or ¼ for p4, and ½, ⅓, or ⅙ for p6 symmetries, respectively. Appropriate building blocks for a $p22_12_1$ unit cell are displayed in Fig. A1 *D* and *E*.

TABLE A2 Geometric forms of partially self-contained two-dimensional crystals of biological macromolecules

Plane group	Symmetry	Cylinder	Cone angles: undistorted	Cone angles: flattened	Number of forms possible
$p1$	p1	++*	—		1
$p12$	pm	++	—		1
$p12_1$	pg	++	—		1
$c12$	cm	++	—		1
$p21$	p2	++	60°*	90°	2
$p222$	pmm	++	60°	90°	2
$p21_12$	pmg	++	60°‡§	90°	2
$p22_12_1$	pgg	++	60°‡§	90°	2
$c222$	cmm	++	60°§	90°	2
$p3$	p3	+*	38.94°	60°	3
			83.62°	120°	—
$p312$	p3m1	+	same as $p3$		3
$p321$	p31m	+	same as $p3$		3
$p4$	p4	+	28.96°‖	45°	4
			60°	90°	—
			97.18°‖	135°	—
$p422$	p4m	+	28.96°‖	45°	4
			60°§	90°	—
			97.18°‖	135°	—
$p42_12$	p4g	+	same as $p422$		4
$p6$	p6	+	19.19°‖	30°	6
			38.94°‖	60°	—
			60°	90°	—
			83.62°‖	120°	—
			112.89°‖	150°	—
$p622$	p6m	+	same as $p6$		6

*With plane groups $p1$ to $c222$, two different lattice dimensions a and b exist such that two nonequivalent types of cylinders (and cones) can be constructed (indicated by $^{++}$). With plane groups $p3$ to $p622$ $b = a$ and all cylinders possible and cones possessing identical angles are of the same type (indicated by $^{+}$). ‡Only possible if the building block is a dimer or a monomer (see Fig. A1). Using the (presumably unlikely) unit shown in Fig. A1 *B* only one type of cone can be formed. §Impossible if a building block equivalent to that shown in Fig. A1 *C* is used. ‖Impossible if a building block of unit cell size and possessing a local two-fold symmetry axis (equivalent to that shown in Fig. A1 *F*) is used.

There may, however, be restrictions if the building blocks are of unit cell size (e.g., Fig. A1 *B*) and, particularly, if they possess a local two-fold symmetry axis like those shown in Fig. A1 *C* and *F*. Now, only some or even none of the cones can be formed (Table A2). In any case, however, the construction of cylinders is feasible.

Interestly, cones like those observed with the reconstituted surface protein of *C. acidovorans* (A10) have not been found in natural systems as yet. A possibility one could think of is the formation of cone-shaped poles of rodlike cells. But there is a significant drawback of putting cylinders and cones together, i.e., the crystal boundaries do not fit and create a ringlike zone of lattice discontinuity. But disclinations, indeed, play a role in forming the pole caps of rodlike cell envelopes as revealed by the analysis of the surface layer from *Thermoproteus tenax* (A14, A15). Disclinations, i.e., predominantly 60° disclinations with the p6 lattice, are introduced at the ends of the cylindrical envelope, reducing its diameter and forming apparently completely protein-

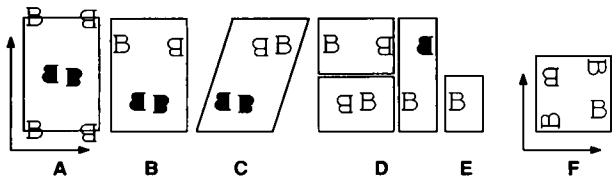

FIGURE A1 Building blocks of unit cell size or smaller of the two-sided plane group $p22_12_1$ (*A–E*). The symbol *B* represents a chiral (biological) molecule (or asymmetric unit). ◧ denotes the upside down orientation of *B* with respect to the x,y-plane, unit cell symbols adapted from Hovmöller (A12). Equivalent building blocks may be obtained by rotation around the *z*-axis (normal to the plane) or around one of the axes (*x* or *y*) lying within the plane; these units are not displayed. (*A*) Crystallographic unit cell, (*B*) building block of unit cell dimensions (presumably unlikely because of nonequivalent dimeric forms occuring in one complex), (*C*) building block of unit cell size, (*D*) different types of (dimeric) building blocks with half of the unit cell size, (*E*) monomeric building block, i.e., the smallest possible, (*F*) building block of unit cell size with a local axis of two-fold symmetry (here plane group *p*4 with unit cell dimensions $b = a$).

covered pole caps. This principle might also apply for the surface layers of the related species listed in Table A1. The formation of tapering ends found with, e.g., the gas vesicles, might however, be an effect of dislocations rather than of disclinations.

APPENDIX REFERENCES

A1. Baumeister, W., and H. Engelhardt. 1987. Three-dimensional structure of bacterial surface layers. *In* Electron Microscopy of Proteins Vol. 6. Membranous Structures. J. R. Harris and R. W. Horne, editors. Academic Press, London. 109–154.

A2. Baumeister, W., I. Wildhaber, and W. Baumeister. 1989. Principles of organization in eubacterial and archaebacterial surface proteins. *Can. J. Microbiol.* 35:215–227.

A3. Sleytr, U. B., and P. Messner. 1983. Crystalline surface layers on bacteria. *Annu. Rev. Microbiol.* 37:311–339.

A4. Chalcroft, J. P., H. Engelhardt, and W. Baumeister. 1987. Structure of the porin from a bacterial stalk. *FEBS (Fed. Eur. Biochem. Soc.) Lett.* 211:53–58.

A5. Kessel, M., M. Radermacher, and J. Frank. 1985. The structure of the stalk surface layer of a brine pond microorganism: correlation averaging applied to a double layered lattice structure. *J. Microscopy (Oxford).* 139:63–74.

A6. Rachel, R., A. M. Engel, R. Huber, K.-O. Stetter, and W. Baumeister. 1990. A porin-type protein is the main constituent of the cell envelope of the ancestral eubacteriaum *Thermotoga maritima. FEBS (Fed. Eur. Biochem. Soc.) Lett.* 262:64–68.

A7. Engelhardt, H., W. Baumeister, and W. O. Saxton. 1983. Electron microscopy of photosynthetic membranes containing bacteriochlorophyll b. *Arch. Microbiol.* 135:169–175.

A8. Baumeister, W., F. Karrenberg, R. Rachel, A. Engel, B. Ten Heggeler, and W. O. Saxton. 1982. The major cell envelope protein of *Micrococcus radiodurans* (R1). Structural and chemical characterization. *Eur. J. Biochem.* 125:535–544.

A9. Messner, P., D. Pum, and U. B. Sleytr. 1986. Characterization of the ultrastructure and the self-assembly of the surface layer of *Bacillus stearothermophilus* strain NRS 2004/3a. *J. Ultrastruct. Mol. Res.* 97:73–88.

A10. Paul, A., H. Engelhardt, U. Jakubowski, and W. Baumeister. 1991. Two-dimensional crystallization of a bacterial surface protein on lipid vesicles under controlled conditions. *Biophys. J.* 61:172–188.

A11. Bohsung, J., and H.-R. Trebin. 1989. Defects in quasicrystals. *In* Aperiodicity and Order. Vol. 2. Introduction to the mathematics of quasicrystals. M. V. Jaric, editor. Academic Press, Boston. 183–221.

A12. Hovmöller, S. 1986. Three-dimensional structure of membrane proteins. *In* Techniques for the Analysis of Membrane Proteins. C. I. Ragan and R. J. Cherry, editors. Chapman and Hall, London. 315–344.

A13. Engelhardt, H. 1988. Correlation averaging and 3-D reconstruction of 2-D crystalline membranes and macromolecules. *Methods Microbiol.* 20:357–413.

A14. Messner, P., D. Pum, M. Sára, K. O. Stetter, and U. B. Sleytr. 1986. Ultrastructure of the cell envelope of the archaebacteria *Thermoproteus tenax* and Thermoproteus neutrophilius. J. Bacteriol. 166:1046–1054.

A15. Wildhaber, I., and W. Baumeister. 1987. The cell envelope of *Thermoproteus tenax:* three-dimensional structure of the surface layer and its role in shape maintenance. *EMBO (Eur. Mol. Biol. Organ.) J.* 6:1475–1480.

A16. Phipps, B. M., H. Engelhardt, R. Huber, and W. Baumeister. 1990. Three-dimensional structure of the crystalline protein envelope layer of the hyperthermophilic archaebacterium *Pyrobaculum islandicum. J. Struct. Biol.* 103:152–163.

A17. Phipps, B. M., R. Huber, W. Baumeister. 1991. The cell envelope of the hyperthermophilic archaebacteriaum *Pyrobaculum organotrophum* consists of two regularly arrayed protein layers: three-dimensional structure of the outer layer. *Mol. Microbiol.* 5:253–265.

A18. Stewart, M., T. J. Beveridge, and G. D. Sprott. 1985. Crystalline order to high resolution in the sheath of *Methanospirillum hungatei:* a cross-beta structure. *J. Mol. Biol.* 183:509–515.

A19. Patel, G. B., G. D. Sprott, R. W. Humphrey, and T. J. Beveridge. 1986. Comparative analyses of the sheath structures of *Methanothrix concilii* GP6 and *Methanospirillum hungatei* strains GP1 and JF1. *Can. J. Microbiol.* 32:623–631.

A20. Smit, J., D. A. Grano, R. M. Glaeser, and N. Agabian. 1981. Periodic surface array in *Caulobacter crescentus:* fine structure and chemical analysis. *J. Bacteriol.* 146:1135–1150.

A21. Elmes, M. L., D. G. Scraba, and J. H. Weiner. 1986. Isolation and characterization of the tubular organelles induced by fumarat reductase overproduction in *Escherichia coli. J. Gen. Microbiol.* 132:1429–1439.

A22. Easterbrook, K. B., J. H. M. Willison, and R. W. Coombs. 1976. Arrangement of morphological subunits in bacterial spinae. *Can. J. Microbiol.* 22:619–629.

A23. Blaurock, A. E., and A. E. Walsby. 1976. Crystalline structure of the gas vesicle wall from *Anabaena flos-aquae. J. Mol. Biol.* 105:183–199.

A24. Bonch-Osmolovskaya, E. A., M. L. Miroshnichenko, N. A. Kostrikina, N. A. Chernych, and G. A. Zavarzin. 1990. *Thermoproteus uzoniensis* sp. nov., a new extremely thermophilic archaebacterium from Kamchatka continental hot springs. *Arch. Microbiol.* 154:556–559.

A25. Shaw, P. J., G. J. Hills, J. A. Henwood, J. E. Harris, and D. B. Archer. 1985. Three-dimensional architecture of the cell

sheath and septa of *Methanospirillum hungatei, J. Bacteriol.* 161:750–757.

A26. Touzel, J. P., G. Prensier, J. L. Roustan, I. Thomas, H. C. Dubourguier, and G. Albagnac. 1988. Description of a new strain of *Methanothrix soehngenii* and rejection of *Methanothrix concilii* as a synonym of *Methanothrix soehngenii. Int. J. Syst. Bacteriol.* 38:30–36.

A27. Hayes, P. K. 1988. Gas vesicles: chemical and physical properties. *Methods Enzymol.* 167:213–222.

We thank our colleague Thomas Hartmann for stimulating discussions and Markus Schaumberger for his help with the development of computer programs.

The work was supported by grants of the Deutsche Forschungsgemeinschaft, projects B5 and D4 of the Sonderforschungsbereich 266.

Received for publication 24 April 1991 and in final form 17 September 1991.

REFERENCES

1. Henderson, R., J. M. Baldwin, T. A. Ceska, F. Zemlin, E. Beckmann, and K. H. Downing. 1990. Model for the structure of bacteriorhodopsin based on high-resolution electron cryo-microscopy. *J. Mol. Biol.* 213:899–929.
2. Sass, H. J., G. Büldt, E. Beckmann, F. Zemlin, M. van Heel, E. Zeitler, J. P. Rosenbusch, D. L. Dorset, and A. Massalski. 1989. Densely packed β-structure at the protein-lipid interface of porin is revealed by high-resolution cryo-electron microscopy. *J. Mol. Biol.* 209:171–175.
3. Jap, B. K., K. H. Downing, and P. J. Walian. 1990. Structure of PhoE porin in projection at 3.5 Å resolution. *J. Struct. Biol.* 103:57–63.
4. Kühlbrandt, W., and D. N. Wang. 1991. Three-dimensional structure of plant light-harvesting complex determined by electron crystallography. *Nature (Lond.).* 350:130–134.
5. Boekema, E. J. 1990. The present state of two-dimensional crystallization of membrane proteins. *Electron Microsc. Rev.* 3:87–96.
6. Engelhardt, H. 1991. Electron microscopy of microbial cell wall proteins. Surface topography, three-dimensional reconstruction and strategies for two-dimensional crystallization. *In* Fungal Cell Wall and Immune Response. J.-P. Latgé and D. Boucias, editors. NATO ASI Series, Vol. H53. Springer-Verlag, Berlin, 11–25.
7. Skriver, E., A. B. Maunsbach, and P. L. Jorgensen. 1981. Formation of two-dimensional crystals in pure membrane-bound Na^+, K^+-ATPase. *FEBS (Fed. Eur. Biochem. Soc.) Lett.* 131:219–222.
8. Mannella, C. A. 1984. Phospholipase-induced crystallization of channels in mitochondrial outer membranes. *Science (Wash. DC).* 224:165–166.
9. Seki, S., H. Hayashi, and T. Oda. 1970. Studies on cytochrome oxidase. Fine structure of cytochrome oxidase-rich submitochondrial membrane. *Arch. Biochem. Biophys.* 138:110–121.
10. Wingfield P., T. Arad, K. Leonard, and H. Weiss. 1979. Membrane crystals of ubiquinone: cytochrome *c* reductase from *Neurospora* mitochondria. *Nature (Lond.).* 280:696–697.
11. Singer, S. J. 1990. The structure and insertion of integral proteins in membranes. *Annu. Rev. Cell Biol.* 6:247–296.
12. Engel, A., A. Massalski, H. Schindler, D. L. Dorset, and J. P. Rosenbusch. 1985. Porin channel triplets merge into single outlets in *Escherichia coli* outer membranes. *Nature (Lond.).* 317:643–645.
13. Mannella, C. A. 1989. Structure of the mitochondrial outer membrane channel derived from electron microscopy of two-dimensional crystals. *J. Bioenerg. Biomembr.* 21:427–437.
14. Deisenhofer, J., O. Epp, K. Miki, R. Huber, and H. Michel. 1985. Structure of the protein subunits in the photosynthetic reaction centre of *Rhodopseudomonas viridis* at 3 Å resolution. *Nature (Lond.).* 318:618–624.
15. Henderson, R., and P. N. T. Unwin. 1975. Three-dimensional model of purple membrane obtained by electron microscopy. *Nature (Lond.).* 257:28–32.
16. Stankovic, C. J., S. H. Heinemann, J. M. Delfino, F. J. Sigworth, and S. L. Schreiber. 1989. Transmembrane channels based on tartaric acid-gramicidin A hybrids. *Science (Wash. DC).* 244:813–817.
17. Dempsey, C. E. 1990. The actions of melittin on membranes. *Biochim. Biophys. Acta.* 1031:143–161.
18. Rabon, E. C., and M. A. Reuben. 1990. The mechanism and structure of the gastric H,K-ATPase. *Annu. Rev. Physiol.* 52:321–344.
19. Taylor, K. A., L. Dux, and A. Maronosi. 1986. Three-dimensional reconstruction of negatively stained crystals of the CA^{2+}-ATPase from muscle sarcoplasmic reticulum. *J. Mol. Biol.* 187:417–427.
20. Hebert, H., E. Skriver, and A. B. Maunsbach. 1985. Three-dimensional structure of renal Na,K-ATPase determined by electron microscopy of membrane crystals. *FEBS (Fed. Eur. Biochem. Soc.) Lett.* 187:182–186.
21. Unwin, N. P. T., C. Toyoshima, and E. Kubalek. 1988. Arrangement of the acetylcholine receptor subunits in the resting and desensitized states, determined by cryoelectron microscopy of crystallized Torpedo post-synaptic membranes. *J. Cell Biol.* 107:1123–1138.
22. Fischetti, V. A., V. Pancholi, and O. Schneewind. 1990. Conservation of a hexapeptide sequence in the anchor region of surface proteins from Gram-positive cocci. *Mol. Microbiol.* 4:1603–1605.
23. Baumeister, W., I. Wildhaber, and B. M. Phipps. 1989. Principles of organization in eubacterial and archaebacterial surface proteins. *Can. J. Microbiol.* 35:215–227.
24. Hynes, R. O. 1987. Integrins: A family of cell surface receptors. *Cell.* 48:549–554.
25. Sefton, B. M., and J. E. Buss. 1987. The covalent modification of eukaryotic proteins with lipid. *J. Cell Biol.* 104:1499–1453.
26. Schmidt, M. F. G. 1983. Fatty acid binding: a new kind of posttranslational modification of membrane proteins. *Curr. Top. Microbiol. Immunol.* 102:101–129.
27. Cross, G. A. M. 1990. Glycolipid anchoring of plasma membrane proteins. *Annu. Rev. Cell Biol.* 6:1–39.
28. Ferguson, M. A. J. 1988. Cell-surface anchoring of proteins via glycosyl-phosphatidylinositol structures. *Annu. Rev. Biochem.* 57:285–320.
29. Engelhardt, H., S. Gerbl-Rieger, D. Krezmar, S. Schneider-Voss, A. Engel, and W. Baumeister. 1990. Structural properties of the outer membrane and the regular surface protein of *Comamonas acidovorans. J. Struct. Biol.* 105:92–102.
30. Engelhardt, H., S. Gerbl-Rieger, U. Santarius, and W. Baumeis-

ter. 1991. The three-dimensional structure of the regular surface protein of *Comamonas acidovorans* derived from native outer membranes and reconstituted two-dimensional crystals. *Mol. Microbiol.* 5:1695–1702.

31. Engel, A., A. Holzenburg, K. Stauffer, J. Rosenbusch, and U. Aebi. 1988. A novel reconstitution method for inducing the formation of regular two-dimensional arrays of membrane proteins and lipids. *In* Proc. 46th Annual Meeting of Electron Microscopy Society America. G. W. Bailey, editor. San Francisco Press, San Francisco. 152–153.
32. Tamaoka, J., D.-M. Ha, and K. Komagata. 1987. Reclassification of *Pseudomonas acidovorans* den Dooren de Jong 1926 and *Pseudomonas testosteroni* Marcus and Talalay 1956 as *Comamonas acidovorans* comb. nov. and *Comamonas testosteroni* comb. nov., with an amended description of the genus *Comamonas*. *Int. J. Syst. Bacteriol.* 37:52–59.
33. Chalcroft, J. P., H. Engelhardt, and W. Baumeister. 1986. Three-dimensional structure of a regular surface layer from *Pseudomonas acidovorans*. *Arch. Microbiol.* 144:196–200.
34. Smith, P. K. R. I. Krohn, G. T. Hermanson, A. K. Mallia, F. H. Gartner, M. D. Provenzano, E. K. Fujimoto, N. M. Goeke, B. J. Olson, and D. C. Klenk. 1985. Measurement of protein using bicinchoninic acid. *Anal. Biochem.* 150:76–85.
35. Rachel, R., U. Jakubowski, H. Tietz, R. Hegerl, and W. Baumeister. 1986. Projected structure of the surface protein of *Deinococcus radiodurans* determined to 8 Å resolution by cryomicroscopy. *Ultramicroscopy.* 20:305–316.
36. Jakubowski, U., and M. Mende. 1991. Preparation of ultrathin amorphous ice films for cryo-electron microscopy. *J. Microscopy (Oxford).* 161:241–252.
37. Saxton, W. O., and W. Baumeister. 1982. The correlation averaging of a regularly arranged bacterial cell envelope protein. *J. Microscopy (Oxford).* 127:127–138.
38. Saxton, W. O., T. J. Pitt, and M. Horner. 1979. Digital image processing: The SEMPER system. *Ultramicroscopy.* 4:343–354.
39. Kerker, M. 1969. The scattering of light. Academic Press, New York.
40. Foitzik, L., and H. Hinzpeter. 1958. Sonnenstrahlung und Lufttrübung. Akademische Verlagsgesellschaft Geest and Portig K.-G., Leipzig.
41. Baumeister, W., and H. Engelhardt. 1987. Three-dimensional structure of bacterial surface layers. *In* Electron microscopy of proteins. Vol. 6. Membranous structures. J. R. Harris and R. W. Horne, editors. Academic Press, London. 109–154.
42. Kühlbrandt, W. 1984. Three-dimensional structure of the light-harvesting chlorophyll a/b-protein complex. *Nature (Lond.).* 307:478–480.
43. Lyon, M. K., and P. N. T. Unwin. 1988. Two-dimensional structure of the light-harvesting chlorophyll a/b complex by cryoelectron microscopy. *J. Cell Biol.* 106:1515–1523.
44. Miller, K. R., and J. S. Jacob. 1983. Two-dimensional crystals formed from photosynthetic reaction centers. *J. Cell Biol.* 97: 1266–1270.
45. Uzgiris, E. E., and R. D. Kornberg. 1983. Two-dimensional crystallization technique for imaging macromolecules, with application to antigen-antibody-complement complexes. *Nature (Lond.).* 301:125–129.
46. Harris, J. R. 1982. The production of paracrystalline two-dimensional monolayers of purified protein molecules. *Micron.* 13:147–168.
47. Milsmann, M. H. W., R. A. Schwendener, and H.-G. Weder. 1978. The preparation of large single bilayer liposomes by a fast and controlled dialysis. *Biochim. Biophys. Acta.* 512:147–155.
48. Aden, A. L., and M. Kerker. 1951. Scattering of electromagnetic waves from two concentric spheres. *J. Appl. Phys.* 22:1242–1246.
49. Rhoden, V., and S. M. Goldin. 1979. Formation of unilamellar lipid vesicles of controllable dimensions by detergent dialysis. *Biochemistry.* 18:4173–4176.
50. Rosenbusch, J. P. 1990. The critical role of detergents in the crystallization of membrane proteins. *J. Struct. Biol.* 104:134–138.
51. Chang, C.-F., S. Mizushima, and R. M. Glaeser. 1985. Projected structure of the pore-forming OmpC protein from *Escherichia coli* outer membrane. *Biophys. J.* 47:629–639.
52. Hovmöller, S., M. Slaughter, J. Berriman, B. Karlsson, H. Weiss, and K. Leonard. 1983. Structural studies of cytochrome reductase. *J. Mol. Biol.* 165:401–406.
53. Lipowsky, R. 1991. The conformation of membranes. *Nature (Lond.).* 349:475–481.
54. Bohsung, J., and H.-R. Trebin. 1989. Defects in quasicrystals. *In* Aperiodicity and order, Vol. 2. Introduction to the mathematics of quasicrystals. Academic Press, San Diego. 183–221.